MSc in Photonics

PHOTONICS**BCN**

Universitat Politècnica de Catalunya (UPC)
Universitat Autònoma de Barcelona (UAB)
Universitat de Barcelona (UB)
Institut de Ciències Fotòniques (ICFO)

http://www.photonicsbcn.eu

Master in Photonics

MASTER THESIS WORK

Holographic imaging of nanometer-scale phase-separation during a phase transition

Jordi Valls Conesa

Supervised by Prof. Dr. Simon Wall, ICFO

Presented on date 9th September 2019

Registered at

Escola Tècnica Superior d'Enginyeria de Telecomunicació de Barcelona

Holographic imaging of nanometer-scale phase-separation during a phase transition

Jordi Valls Conesa
September 2019
Advisor: Prof. Dr. Simon Wall
Affilation: UDQS group, ICFO

E-mail: jordiv1996.jv@gmail.com

Abstract. Quantum materials is a broad term used in condensed matter physics to define materials whose collective properties are governed by quantum behavior, which are challenging to understand. These materials are sensitive to small changes in the environment,such as changes in temperature, doping or strain. This can lead to nanoscale phase separation, in which a single sample can coexist different states at different regions of space. In this thesis, a method for imaging this phase separation based on coherent diffractive imaging is developed and is applied to the quantum material VO_2.

Keywords: Vanadium dioxide, Fourier Transform Holography, Coherent Diffraction Imaging, Iterative Phase Reconstruction

1. Introduction

1.1. The phases of VO_2

VO_2 is a quantum material that exhibits a metal-insulator transition as a function of temperature. For temperatures bellow the critical temperature of the transition, $T_c \approx 340$ K [1], VO_2 presents a monoclinic M_1 structure (insulator phase). Above T_c VO_2 undergoes a first order transition into a metallic phase with a rutile crystal R structure.

While the insulator-to-metal phase transformation is the most studied, the application Cr-doped or uniaxial strains along *c*-axis led to the discover of two other insulating states besides M_1, a second monoclinic structure M_2 and a triclinic structure T [2]. The different phase transitions are represented in Fig.(1) as a function of strain and temperature. As only moderate strains are required to change the phase, VO_2 samples can easily switch between the different phases. In devices, where the strain may not be homogeneous, this can lead to different phases coexisting.

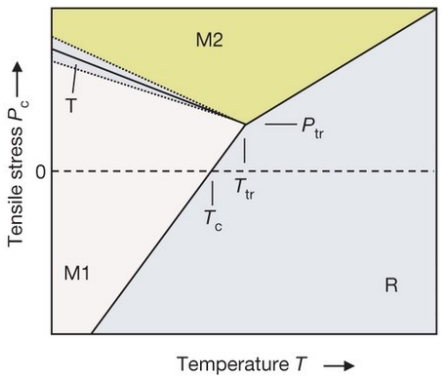

Figure 1: The phase map that correspond to the possible phases depending on the stress and temperature. [2]

1.2. VO_2 XAS specta

In order to observe this phase separation two conditions need to be met. Firstly, the images require nanometer spatial resolution and the second is to achieve a method to contrast the different phases.

Resonant soft X-ray holography is a tool that can achieve both criteria. This method uses soft X-ray tuned to the absorption resonances of the oxygen K edge, which has been shown to be sensitive to the structural and electronic transition.

In the XAS spectrum of VO_2 (Fig. (2)) at 529 eV there is a main peak present in both phases that shows a small red-shift on entering the metallic phase (with strain in the crystal this peak shows the presence of M_2). At 532 eV there is a second peak corresponding to a band that is above the Fermi level and, thus, do not present any variation in the phase transition. Between these two peaks there is a third peak at 530.5 eV that is only observable in the insulating phase, which arise from the structural change in the insulating phase.

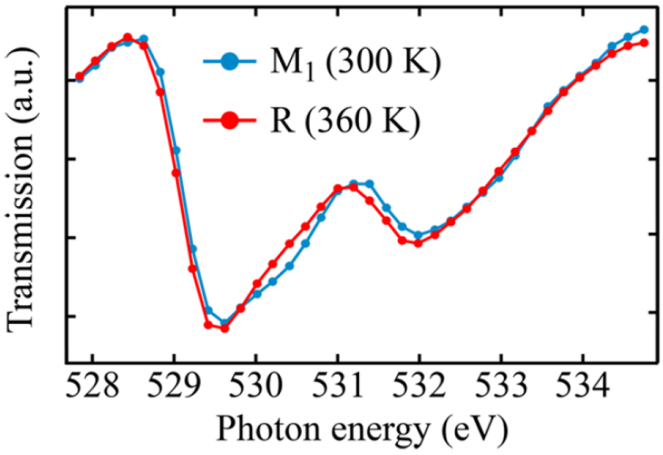

Figure 2: X-ray transmission spectra of VO_2 at the O K edge, measured at low (300 K) and high (360 K) temperatures. These spectra show the difference between the metal and insulator phases [3].

1.3. Soft X-rays Fourier Transform Holography

Fourier Transform Holography (FTH) [4] is a lensless imaging technique that belongs to a group of techniques called Coherent Diffraction Imaging (CDI), which aim to reproduce real space nanoscale images from diffraction data alone, without the need for optical components. For lensless CDI the system consist of coherent X-rays, a sample and a detector. When the coherent X-ray light crosses a thin sample the light is transmitted and diffracted. The detector is located a certain distance along axis z from the sample. If z is sufficiently far that we are in the far field limit, the diffracted wave can be described by the Fraunhofer diffraction approximation [4]

$$\psi(X,Y) = \frac{e^{(ikz)}}{iz\lambda} e^{\left(i\frac{k}{2z}[X^2+Y^2]\right)} \int\int_{-\infty}^{\infty} \psi(x,y) e^{\left(-i\frac{k}{z}[xX+yY]\right)} \mathrm{d}x\mathrm{d}y, \tag{1}$$

where $\psi(x,y)$ is the exit wave at the sample plane, λ is the wavelength of the light k is the wave-vector, x and y are the coordinates of the samples plane and X and Y are the coordinates of the detectors plane. This wave propagation is the standard expression for a Fourier transform where the spatial frequencies are $k_x = X/z\lambda$ and $k_y = Y/z\lambda$ for a reciprocal space (k_x, k_y).

However, detectors are only able to measure intensity $I(k_x,k_y) = |\psi(k_x,k_y)|^2$, thus the phase of the retrieved image is completely lost, this is the phase problem [4] since a real-space image of the object cannot be obtained from the amplitude information alone. The intensity will have the mathematical form

$$I(k_x,k_y) = \frac{1}{z^2\lambda^2} \left| \int\int_{-\infty}^{\infty} \psi(x,y) e^{\left(-i2\pi[xk_x+yk_y]\right)} \mathrm{d}x\mathrm{d}y \right|^2, \tag{2}$$

subtracting all the exponential of an imaginary terms. To solve the phase problem, one solution is to apply FTH by placing a reference at the same plane as the object. This way it is possible to encode the phase information in intensity modulations, the interference pattern obtained after adding a mask is the so called hologram. The detected intensity in the far field conditions is defined by the object of interest $o(x, y)$ and the known reference $r(x - x_0, y - y_0)$, given by

$$H(k_x, k_y) = \left|\mathcal{F}\left[o(x, y) + r(x - x_0, y - y_0)\right]\right|^2, \tag{3}$$

with $O(k_x, k_y)$ and $R(k_x, k_y)e^{-i(k_x x_0 + k_y y_0)}$ as the Fourier transforms of $o(x, y)$ and $r(x - x_0, y - y_0)$ respectively, the hologram intensity can be expressed as

$$\begin{aligned} H(k_x, k_y) = |O(k_x, k_y)|^2 + |R(k_x, k_y)|^2 + O(k_x, k_y)R^*(k_x, k_y)e^{i(k_x x_0 + k_y y_0)} + \\ + O^*(k_x, k_y)R(k_x, k_y)e^{-i(k_x x_0 + k_y y_0)}. \end{aligned} \tag{4}$$

The reconstruction of the object's exit wave can now be found by applying digitally an inverse Fourier transform to the hologram

$$\begin{aligned} \mathcal{F}\left(H(k_x, k_y)\right) = o(x, y) \otimes o^*(-x, -y) + r(x, y) \otimes r^*(-x, -y) + \\ + o(x + x_0, y + y_0) \otimes r^*(-x, -y) + r(x, y) \otimes o^*(-x - x_0, -y - y_0), \end{aligned} \tag{5}$$

where $\otimes$ represents a convolution.

For the analyzed samples, the reference has a point-like shape, and thus can be represented as a Dirac δ-distribution at $\delta(x - x_0, y - y_0)$. The inverse Fourier transform of the hologram can be rewritten as

$$\begin{aligned} \mathcal{F}\left(H(k_x, k_y)\right) = o(x, y) \star o(x, y) + \delta(x, y) + o(x + x_0, y + y_0) + \\ + o^*(-x - x_0, -y - y_0), \end{aligned} \tag{6}$$

where $\star$ represents a correlation.

The distance between the object and the reference $d = (x_0, y_0)$ has to be large enough for the object to be spatially separated from the region of the autocorrelation of the object. The radius of the object is r_{obj} and thus the radius of its autocorrelation is $2r_{obj}$, then the separation between the reference and the object shall be $d \geq 3r_{obj}$. Instead of working with one reference, the sample had three references, this way, in the reconstruction using the FTH, appear three objects and its complex conjugates, making the analysis easier and increasing the signal to noise ratio.

1.4. Real space imaging

The transmittance of a thin sample at wavelength λ, index of refraction $\tilde{n} = n + i\kappa$ and sample thickness d is represented as [5]

$$T(x, y) = \exp\left[i\frac{2\pi}{\lambda}\int_0^d \{\tilde{n}(x, y, z) - 1\}\mathrm{d}z\right]. \tag{7}$$

For the limit of weak contrast $d \sim \lambda$, the equation of the intensity for Eq.(7) is simplified to

$$I(x, y) \approx I_0\left[1 + \frac{2\pi d}{\lambda}(in - \kappa)\right], \tag{8}$$

This equation shows that the transmission of the sample (defined by κ) corresponds to the real component of the of the measured intensity, this way the final image is the real part of the reconstructed hologram using FTH, instead of using the absolute value.

2. Sample preparation and analysis

The sample of VO_2, illustrated in Figure.(3), is a 75-nm-thick sample. And the experiments were made at the UE52-SGM undulation beamline of the BESSY II synchrotron radiation source. For this thesis the data used is the same used at reference [3].

Figure 3: SEM image of the sample of VO_2 used in this thesis. Field of view is 2 μm in diameter. [3]

The maximum pixel resolution is set by the distance between sample and detector (D), wavelength (λ) and the number of pixels (N) and pixel size (ω). Thus, the resolution is given by

$$\delta = \frac{\lambda D}{N\omega}. \tag{9}$$

The maximum spatial resolution can be found as 35 nm, using the data provided by reference [3] and calculated using Eq.(9). Although in reality the resolution of the final object is more limited by the exact experimental conditions.

3. Sample data processing

The data obtained with the synchrotron is composed by images of the hologram created by the diffraction of light from the sample and reference holes. This hologram will be composed of Airy discs because of the sample has a circular shape and with some interferences due to the reference holes. The multiple images will be taken for a range of energies of the incoming light, between 510 eV and 535 eV and for different temperatures of the sample (300 K, 320 K, 330 K, 333 K, 336 K, 341 K, 346 K and 360 K) in order to observe the phase transition.

The exposure time has to be almost $\sim$ 5 s to record the high-frequency regions (high-angle scattering), this also saturates the first Fraunhofer ring (Airy disk) and can potentially damage the CCD, to prevent this a beam-block mask is located in the central part before the CCD producing also a black spot on the central region of the hologram but at the same time the signal to noise ratio (SNR) will be improved for all the hologram, specially at the high frequency regions where the signal is weaker. In the previous work of reference [3], the holograms with a beam-block are the only ones that are used to retrieve the image of the sample. Using just the high frequency region the real part of the image correspond to the transmission image (similar to the images obtained) but without being the absolute transmission of the sample because by ignoring the central region the real value of the intensity is lost.

Another image is taken without the beam-block to obtain the hologram on the low-frequency region, and the exposure time is $\sim$ 0.5 s. This exposure time makes the high-angle scattering too noisy to be reconstructed properly but gives information about the central part. With these two images there is information about all the hologram, then the reconstruction will be similar to other reconstructions of single images [3] with the added condition that now there is the complete information about the sample.

In order to obtain the reconstruction of the hologram the raw data taken by the CCD has to be processed with multiple steps.

- The background of both images is eliminated by using images of the background obtained from recording with the CCD without the X-ray beam.

- The center of the hologram is found and the image is recentered according to these new coordinates. An algorithm for detecting multiple rotational symmetries in natural images [6] is implemented, this algorithm calculates the degree of symmetry by establishing a value to each position where the center may be and finding the center by obtaining the maximum, Instead of finding the center of a rotational symmetry, the algorithm applies the Fourier transform in order to obtain a linearly symmetric system and find the linear symmetry [7].
- The hologram is padded by increasing the number of pixels of the sides. This padding increases the resolution of the reconstructed image after applying the FT.
- A digital mask is applied to the hologram, this mask is a step function with a form of a circle with a Gaussian smothering at the edges (to not find any sharp edge in the transition of the two holograms) centered alongside the hologram. This mask eliminates the central part from the long exposure time hologram, and the inverse of the mask is applied to the short exposure time hologram.
- The low-exposure hologram is multiplied by a factor obtained by comparing both holograms. The two holograms with the masks applied are summed to obtain the whole hologram of the sample with a smooth transition between the two (Fig.(4a)).
- According to Fraunhofer diffraction, the values of the reciprocal space (k_x, k_y) (defined in Eq.(1)) depend on the wavelength ($k_x = X/z\lambda$ and $k_y = Y/z\lambda$) and thus the radius of the rings generated with different wavelengths will have higher radius for higher energies, leading to a shift of the object images in the FTH reconstruction. To compensate the difference of length of the radius, all the images are zoomed (in or out) depending on their energy in comparison with a reference wavelength constant for all energies.
- The hologram is Fourier transformed into the reconstruction of the sample according to Eq.(6), with a correlation in the center and three images of the object and their complex conjugates for each reference, as it is shown in Fig.(4b).

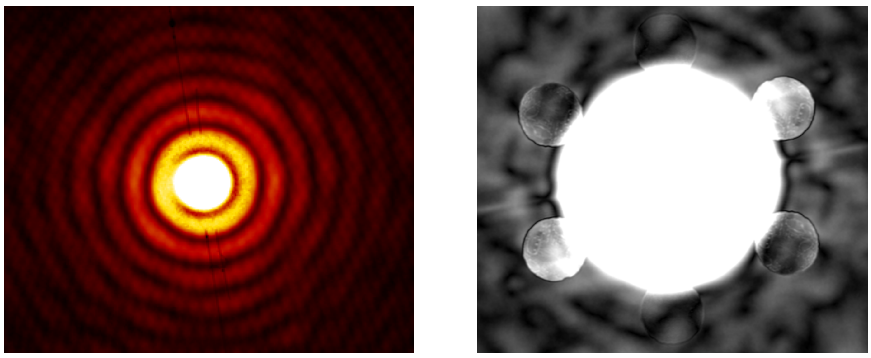

(a) (b)

Figure 4: Images corresponding to a) the square root of the combined holograms and b) Fourier transform of this hologram that shows six images with the sample reconstructed corresponding to the sample at 336 K and the beam energy at 530.5 eV. The high intensity regions have been saturated (white regions) in order to see the low intensity regions like the reconstructed samples in image b).

As it can be seen in Fig.(4b), in the reconstruction of the hologram the sample features can be seen, but there is significant noise and a leakage of the central autocorrelation which makes the intensities obtained meaningless, making impossible a proper extraction of n and κ.

After some research it is found that this is due to the addition of the central region of the hologram, it has an intensity peak in the center that corresponds to incoherent radiation from the

synchrotron (since it is not a perfect coherent light source), another important factor is the visible noise in the middle due to the lower SNR ratio. These two factors lead to an increment of the low frequency noise in the reconstruction, and and also this is added to the problem that one of the top reference hole does not have enough intensity compared to the others, due to the small size of the hole.

With this reconstruction a good image of the sample cannot be retrieved even making an average for all different references. The solution proposed here is to apply another reconstruction method for CDI, apply a iterative phase retrieval algorithm.

4. Beyond FTH

After finding out that FTH alone does not provide a proper reconstruction of the used samples, in this thesis have been developed further methods that compliments FTH to improve the resolution and SNR are applied.

4.1. Iterative phase reconstruction

Phase reconstruction is another CDI method to solve the phase problem. Is different from FTH in the sense that it does not require references to reconstruct the sample, but it can be used in FTH imaging to improve the quality and resolution of the reconstructed sample [8]. In this case, since the sample cannot be correctly reconstructed using FTH an additional phase reconstruction is implemented using an iterative method. The iterative methods used are error reduction (ER), hybrid input-output (HIO) and as a support constraint the shrinkwrap algorithm [9].

Iterative phase retrieval algorithms are reconstruction methods that propagate the complex-valued wavefront between two planes, the CCD plane and the sample plane, considering the intensity of the diffraction pattern and some *a priori* information. The reconstruction is done by applying an iterative procedure of four steps that alternates between the diffraction pattern and its Fourier transform.

The steps that are done ate the k-th iteration are:

(i) Fourier transform of g_k (sample reconstruction), $G_k(k_x, k_y) = \mathcal{F}\left[g_k(x, y)\right]$.

(ii) Application of the Fourier modulus constraint Π_M, $G'_k(k_x, k_y) = \Pi_M\ G_k(k_x, k_y)$.

(iii) Inverse Fourier transform over $G'_k(k_x, k_y)$, $g'_k(x, y) = \mathcal{F}^{-1}\left[G'_k(k_x, k_y)\right]$.

(iv) Application of the support constraint Π_S, $g_{k+1}(x, y) = \Pi_S\ g'_k(x, y)$.

Before the iteration, the wavefront is defined as a combination of the square root of the measured intensity for the absolute part $I(k_x, k_y) = |F(k_x, k_y)|^2$ and the phase is a made up phase that can be random noise or an initial guess based on *a priori* information, in this case the average of the objects reconstructed using FTH plus the reference holes. For CDI the Fourier modulus constrain is always

$$G'_k(k_x, k_y) = \Pi_M\ G_k(k_x, k_y) \rightarrow |F(k_x, k_y)| \exp\left[i\psi_k(k_x, k_y)\right], \tag{10}$$

where $|F(k_x, k_y)|$ is the absolute value of the initial wavefront and $\psi_k(k_x, k_y)$ is the phase of the wavefront at k.

For the support constraint, a support has to be applied using known information that corresponds to the shape of the final object, in this case the shape will correspond to a circle matching the SEM image Fig.(3) and three tiny holes corresponding to the references. The support

(S) will be the set of points at which $g'_k(x,y)$ satisfies the object-domain constraints. For ER the support constraint is

$$g_{k+1}(x,y) = \Pi_S \; g'_k(x,y) \rightarrow \begin{cases} g'_k(x,y), & if(x,y) \in S \\ 0, & if(x,y) \notin S \end{cases}, \tag{11}$$

And for HIO the support constraint is

$$g_{k+1}(x,y) = \Pi_S \; g'_k(x,y) \rightarrow \begin{cases} g'_k(x,y), & if(x,y) \in S \\ g_k(x,y) - \beta g'_k(x,y), & if(x,y) \notin S \end{cases}, \tag{12}$$

where β is typically 0.9.

The shrinkwrap algorithm is a further modification of the iterative phase retrieval algorithm, where the object support S is readjusted during the iterative reconstruction at a defined number of iterations (in this case every 10-th iteration). At the start of the reconstruction the radius of the sample has a higher radius and at the end, the radius matches with the one in Fig.(3) (tight support).

In order to improve the resolution of the reconstruction, an additional mask can be applied in the iteration step (ii). This mask acts like the object support but in this case the step (ii) is only applied at the regions within the mask. This mask is applied in all the diffraction pattern apart from zones with sharp edges, the regions where the string of the beam-block is supported, the ring that corresponds to the connection between the image of low-exposure time and the one of high-exposure time and the outside regions of the padding that are zero, this last one reduces the high frequency noise [10].

The final image using the phase reconstruction process (represented in Fig.(5)) is different from the reconstructed image from FTH, here there is only the reconstructed sample and the three references. The images obtained using this method have better resolution according to the theory. Although the domains can be slightly distinguished, in the appropriate energy, they should not be confused with the crystal defects represented as the white regions.

(a) (b) (c)

Figure 5: Images of the sample reconstructed using CDI Error Reduction, corresponding to the sample at 336 K and the beam with energy a) 529 eV and b) 530.5 eV, and for the sample at c) 320 K and the beam of 530.5 eV. The low frequency noise can be observed as large gradients of intensity different for each sample independently of the temperature or energy.

In these images the high frequency noise has decreased thanks to the implementation of the mask for the iteration step (ii), but by comparing Fig.(5a) and Fig.(5b), it can be seen that there is still low frequency noise that appears because the synchrotron X-ray source is not fully coherent (can easily be observed at the center of Fig.(4a)) and this method only works properly for coherent light. In order to obtain a proper reconstruction of the sample, a different method really similar to the iterative phase reconstruction but considering instead partially-coherent light.

4.2. Partially coherent diffraction imaging

To solve the problem with the coherence of the light from the synchrotron the incoming light is considered partially coherent and cannot be solved with regular CDI reconstruction methods. Despite some papers use methods that require *a priori* information about the coherence of the beam in this case this information is not needed because using an iterative model similar to CDI the coherent part of the beam can be subtracted [11].

The measured partially coherent intensity I_{pc} can be considered as a convolution ($\otimes$) between two components

$$I_{pc}(k_x, k_y) = |F(k_x, k_y)|^2 \otimes \hat{\gamma}(k_x, k_y) = I_{coh}(k_x, k_y) \otimes \hat{\gamma}(k_x, k_y), \tag{13}$$

where $I_{coh}(k_x, k_y)$ is the coherent intensity (and the resulting wavefront $F(k_x, k_y)$ of the iterative method) and $\hat{\gamma}(k_x, k_y)$ is the FT of the complex coherent function. The initial coherence function is an initial guess that can be random noise, a Dirac delta (considering full coherence) but in this case an small Gaussian is taken because is the most similar to the result.

The algorithm is also a phase reconstruction like for the CDI with some differences and additions to accommodate partial coherence. The first difference is that the Fourier modulus constraint for each iteration is no longer the same presented in Eq.(10) for CDI, but a one that compare the partially coherent intensity of each iteration k with the measured intensity following Eq.(13)

$$G'_k(k_x, k_y) = \Pi_M \; G_k(k_x, k_y) \rightarrow G_k(k_x, k_y) \left(\frac{\sqrt{I_{pc}(k_x, k_y)}}{\sqrt{I^k_{pc}(k_x, k_y)}} \right). \tag{14}$$

To obtain the complex coherent function at each step $\gamma^k(k_x, k_y)$ the iterative RichardsonLucy (RL) algorithm is applied. This algorithm updates a numerical estimate of $\gamma^k(k_x, k_y)$ using $I_{pc}(k_x, k_y)$ and a combination of the current and previous iterates estimate of the coherent intensity $I_{\Delta k}(k_x, k_y) = 2I^k_{coh}(k_x, k_y) - I^{k-1}_{coh}(k_x, k_y)$. The iterative scheme for $\hat{\gamma}^k(k_x, k_y)$ is

$$\hat{\gamma}^{k,i+1}(k_x, k_y) = \hat{\gamma}^{k,i}(k_x, k_y) \left(I_{\Delta k}(-k_x, -k_y) \otimes \frac{I_{pc}(k_x, k_y)}{I_{\Delta k}(k_x, k_y) \otimes \hat{\gamma}^{k,i}(k_x, k_y)} \right), \tag{15}$$

where i is the sub iteration of the RL algorithm inside the reconstruction.

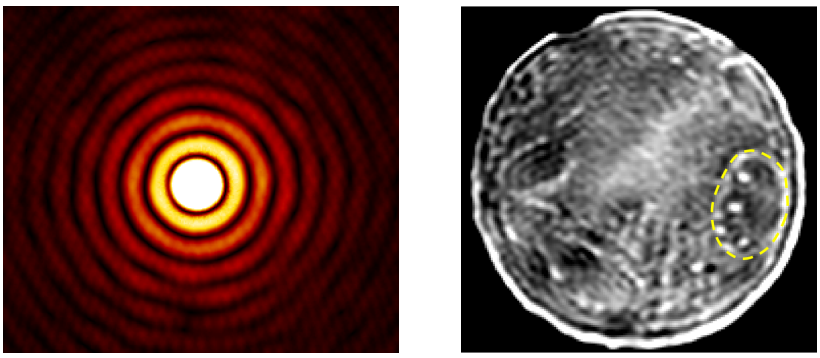

(a) (b)

Figure 6: Images of a) the square root of the coherent hologram and b) the reconstruction of the sample, after the partial coherent reconstruction for the sample at 336 K and a beam energy of 529 eV. Now the noise is been minimized and the crystal domains of the sample can be observed, not only the defects (brighter shapes).

All reconstructions used the same recipe which consisted of 10 iterations of ER, then 1600 iterations of HIO (using $\beta = 0.9$), and then 40 iterations of ER. The support was updated every

fifth iteration using shrinkwrap. The coherence function was updated every 15 iterations with the RL algorithm run for 20 iterations per update. This configuration was found to be adequate to converge to a solution while reducing computation time.

Using this algorithm a coherent hologram can be retrieved (Fig.(6a)) and after applying again the CDI reconstructive method (using shrinkwrap ER of 60 iterations) a reconstructed sample without noise is obtained (Fig.(6b)).

The pixel size of the resulting image of the sample is 12.5 nm each pixel, this means that the size of the pixel is smaller than the resolution (> 35 nm) calculated at Section 2. Implying that the pixel size will not be a limiter for the spatial resolution.

5. Sample analysis

The images retrieved using partially coherent diffraction imaging have enough resolution and a small enough SNR to distinguish the crystal domains at different phases, in particular at the region delimited at Fig.(6b) by a yellow line, that can be seen as not saturated brighter lines. In this image the sample is at 336 K and 529 eV, the domains observed in this image correspond to the M_2 phase. It is needed to point out that the white saturated regions are defects of the crystal that let all the light come through and do not give information about the sample.

In order to observe in further detail the different phases in the region of interest ROI (the region delimited by the yellow dashed line), a RGB image (Fig.(7)) can be done in order to compare the transmission of the sample for different energies of the beam and easily observe the crystal domains. In this case the red is 518 eV (does not correspond to any insulator phase), green is 529 eV (M_2 if strain appear) and blue is 530.5 eV (M_1-R transition), for samples for the same temperature.

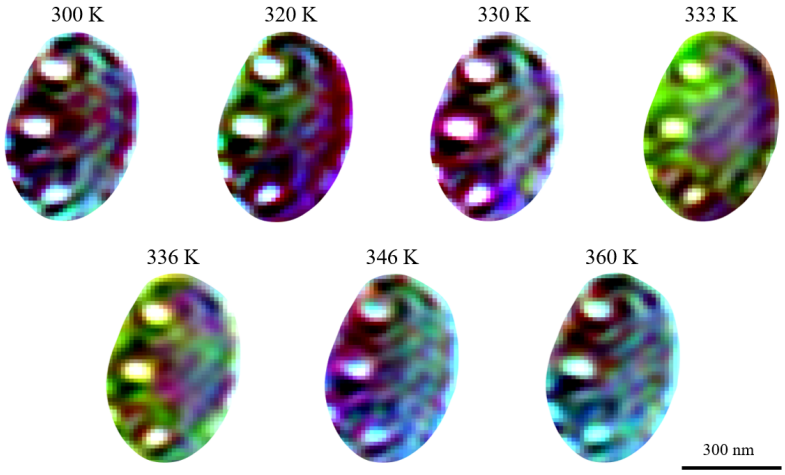

Figure 7: Spectrally resolved images of the ROI of the VO_2 sample for different temperatures. The images are recorded at 518 (red), 529 (green) and 530.5 eV (blue) to encode the intensities of the three color channels of an RGB image. At lower temperatures the color is darker and at higher temperatures the metallic phase prevail. At 333 K and 336 K, green stripes can be observed formed by the M_2 phase.

As it can be seen in the comparison between temperatures at Fig.(7), the M_2 phase generated by strain appears mostly in the sample at 336 K, and the metallic phase is mostly present for temperatures above $\sim$340 K, following the theory.

Another way to observe the domains is comparing using a subtraction to an image of a sample at any temperature where the domains appear (for example 336 K) and another image with a temperature far away from the temperature of the transition (in this case 300 K), represented in

Fig.(8). The result of the subtraction gives information about the crystal domains and without the defects because all the images with the same energy of the beam should have the same shape for the defects.

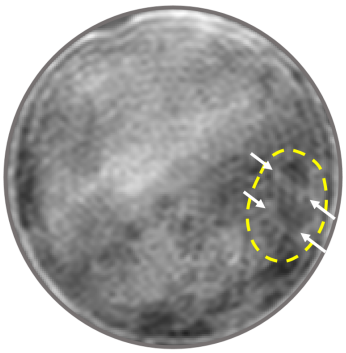

Figure 8: Representation of the subtraction between two samples measured at 529 eV and one at 336 K and the other 300 K. as it can be seen in the image, the defects on the crystals disappeared but de domains can be perfectly seen in the ROI as indicated with the white arrows.

6. Conclusions

In conclusion, this thesis accomplishes the objective of reconstructing a sample using an full hologram reconstructed using a partially coherent method, and nanometer-scale phase separations can be observed in the sample. It is been demonstrated that the resolution and contrast obtained from the reconstruction are enough to observe, distinguish and study the crystal domains. Using the whole hologram implies that the sample shows the original transmitted intensity, this information is relevant for further analysis in spectro-holography. Another important detail is that the iterative reconstructive method is useful for any coherent or partially coherent sample.

A further step after this work is, for example, to obtain the spectra of any point of the sample, to achieve that, the SNR has to be reduced by improving the detection method or with an improved reconstruction method. Another further step can be to retrieve the relation between the incoherence and reconstructed coherence of the hologram, this will also show the real proportion of coherent light coming from the synchrotron.

Acknowledgements: I want to thank Prof. Dr. Simon Wall as well as the whole UDQS group in ICFO for all the support and help that made this thesis possible.

References

[1] Morin, F. J. Oxides which show a metal-to-insulator transition at the neel temperature. *Phys Rev. Lett.* **3,** 34-36 (1959)

[2] Hyung Park, J., Cobden, D. H., *et al.* Measurement of a solid-state triple point at the metal-insulator transition in VO2, *Nature* **500,** 431-4 (2013).

[3] Vidas, L., *et al.* Imaging Nanometer Phase Coexistence at Defects During the Insulator-Metal Phase Transformation in VO2 Thin Films by Resonant Soft Xray Holography, *Nano Lett.* **18,** 3449-3453 (2018).

[4] Gührs, E. Soft X-ray Tomoholography, (2013).

[5] Scherz, A., Schlotter W. F., *et al.* Phase imaging of magnetic nanostructures using resonant soft x-ray holography, *Phys. Rev. B* **76,** 214410 (2007).

[6] Shiv Naga Prasad, V. & Davis, L. S. Detecting Rotational Symmetries, *IEEE Trans. Pattern Anal. Mach. Intell.* **05,** 1550-5499 (2005).

[7] Lee, S. & Liu, Y. Skewed Rotation Symmetry Group Detection, *IEEE Trans. Pattern Anal. Mach. Intell.* **32,** 9 (2010).

[8] Kfir, O., Zayko, *et al.* Nanoscale Magnetic Imaging using Circularly Polarized High-Harmonic Radiation, *Sci. Adv.* **3,** 12 (2017).

[9] Latychevskaia, T. Iterative phase retrieval in coherent diffractive imaging: practical issues, *Appl. Opt.* **57,** 7187-7197 (2018).

[10] Latychevskaia, T., Fink, H.W. Coherent microscopy at resolution beyond diffraction limit using post-experimental data extrapolation, *Appl. Phys. Lett.* **103,** 204105 (2013).

[11] Clark, J. N., *et al.* High-resolution three-dimensional partially coherent diffraction imaging, *Nat. Commun.* **3,** 993 (2012).